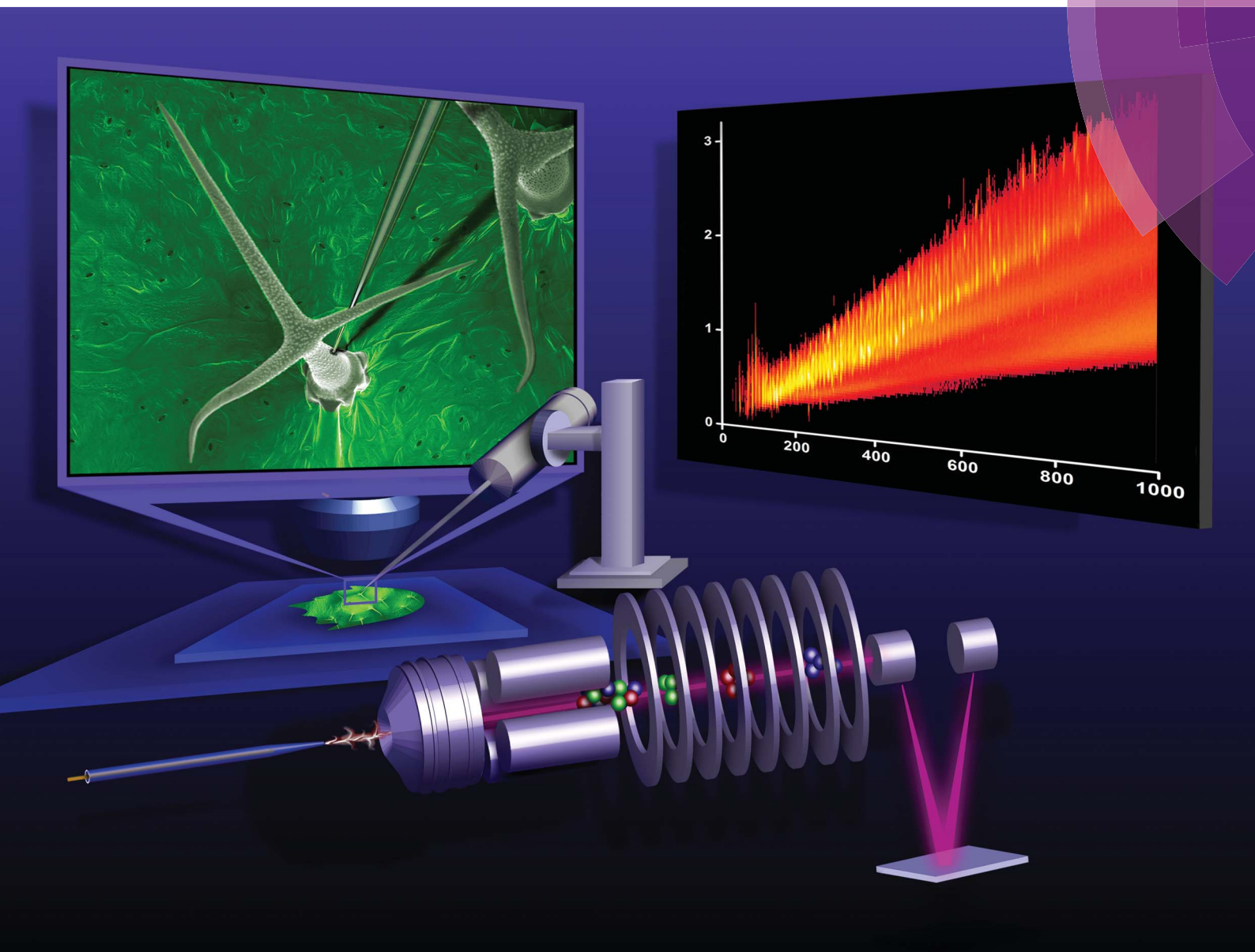


Analyst

www.rsc.org/analyst



ISSN 0003-2654



PAPER

Akos Vertes *et al.*

In Situ metabolic analysis of single plant cells by capillary microsampling and electrospray ionization mass spectrometry with ion mobility separation

CrossMark
click for updatesCite this: *Analyst*, 2014, 139, 5079

In Situ metabolic analysis of single plant cells by capillary microsampling and electrospray ionization mass spectrometry with ion mobility separation†

Linwen Zhang,^a Daniel P. Foreman,^a Paaqua A. Grant,^b Bindesh Shrestha,^a Sally A. Moody,^c Florent Villiers,^d June M. Kwak^e and Akos Vertes^{*a}

Advances in single cell analysis techniques have demonstrated cell-to-cell variability in both homogeneous and heterogeneous cell populations strengthening our understanding of multicellular organisms and individual cell behaviour. However, additional tools are needed for non-targeted metabolic analysis of live single cells in their native environment. Here, we combine capillary microsampling with electrospray ionization (ESI) mass spectrometry (MS) and ion mobility separation (IMS) for the analysis of various single *A. thaliana* epidermal cell types, including pavement and basal cells, and trichomes. To achieve microsampling of different cell types with distinct morphology, custom-tailored microcapillaries were used to extract the cell contents. To eliminate the isobaric interferences and enhance the ion coverage in single cell analysis, a rapid separation technique, IMS, was introduced that retained ions based on their collision cross sections. For each cell type, the extracted cell material was directly electrosprayed resulting in ~200 peaks in ESI-MS and ~400 different ions in ESI-IMS-MS, the latter representing a significantly enhanced coverage. Based on their accurate masses and tandem MS, 23 metabolites and lipids were tentatively identified. Our results indicated that profound metabolic differences existed between the trichome and the other two cell types but differences between pavement and basal cells were hard to discern. The spectra indicated that in all three *A. thaliana* cell types the phenylpropanoid metabolism pathway had high coverage. In addition, metabolites from the subpathway, sinapic acid ester biosynthesis, were more abundant in single pavement and basal cells, whereas compounds from the kaempferol glycoside biosynthesis pathway were present at significantly higher level in trichomes. Our results demonstrate that capillary microsampling coupled with ESI-IMS-MS captures metabolic differences between *A. thaliana* epidermal cell types, paving the way for the non-targeted analysis of single plant cells and subcellular compartments.

Received 4th June 2014

Accepted 26th July 2014

DOI: 10.1039/c4an01018c

www.rsc.org/analyst

Introduction

Single cell metabolomics enables the chemical characterization of cellular states within heterogeneous cell populations. For

example, it can provide insight into cellular function, heterogeneity, and single cell responses to perturbations.^{1,2} *In situ* metabolic analysis of single cells faces significant challenges, such as the low amount of metabolites, the difficulty of handling and extracting small volumes of the sample, the fast metabolic changes due to external perturbations, and the molecular complexity present within a cell.³

To design an approach for molecular analysis of a specific cell type, both the sampling and detection aspects need to be considered. Due to its high sensitivity and specificity, mass spectrometry (MS) is a promising tool for non-targeted metabolic analysis of single cells.⁴ Some MS techniques, such as secondary ion MS (SIMS), matrix-assisted laser desorption/ionization (MALDI) MS, desorption/ionization on porous silicon (DIOS) MS, and laser ionization from silicon nanopost arrays (NAPA), have been developed and employed for single cell analysis under vacuum conditions.^{5–9} Although these

^aDepartment of Chemistry, W. M. Keck Institute for Proteomics Technology and Applications, The George Washington University, Washington, DC 20052, USA. E-mail: vertes@gwu.edu; Fax: +1 (202) 994-5873; Tel: +1 (202) 994-2717

^bDepartment of Biological Sciences, The George Washington University, Washington, DC 20052, USA

^cDepartment of Anatomy and Regenerative Biology, The George Washington University, Washington, DC 20037, USA

^dDepartment of Cell Biology and Molecular Genetics, University of Maryland, College Park, Maryland 20742, USA

^eCenter for Plant Aging Research, Institute for Basic Science, Department of New Biology, Daegu Gyeongbuk Institute of Science and Technology, Daegu 711-873, Republic of Korea

† Electronic supplementary information (ESI) available. See DOI: 10.1039/c4an01018c

techniques have their own unique advantages and applications, they require high vacuum conditions and often elaborate sample preparation steps prior to MS analysis. These protocols may include the isolation of single cells by laser capture microdissection, freeze-fracture sample treatment for SIMS, and matrix treatment of the samples for MALDI. These steps may affect the natural metabolic state of the cells and result in a limited ability to follow temporal changes in the cells.^{10–12}

In recent years, ambient ionization MS techniques that permit rapid sampling and ionization of biological samples in their native environment have been adapted for single cell analysis.¹³ Live single cell MS using a gold-coated nano-electrospray tip to extract single cell contents followed by direct analysis by MS have been established and applied for metabolite analysis of single mammalian cells and their organelles.^{14–16} More recently, drug metabolism in single human hepatic cells was directly monitored by this technique.¹⁷ Mass cytometry, a combination of flow cytometry and MS, has been used for sorting and identification of the suspended mammalian cells.¹⁸ Laser ablation electrospray ionization (LAESI) is demonstrated for metabolic profiling of single plant cells and their subcellular compartments.^{19–22} Whole-cell patch clamp recording and CE-MS have been implemented to measure the physiological activity of single neurons and the metabolite composition in the cytoplasm, respectively.²³

Due to the thousands of molecular species present within a biological tissue, to reduce the complexity of the mass spectra and enhance molecular coverage, a rapid separation step, *e.g.*, ion mobility separation (IMS), may be coupled with ambient ionization MS. Due to its capability to separate isobaric ions within milliseconds after ionization, IMS is a promising choice in combination with ambient ionization methods. For example, IMS-MS utilizing ambient ionization sources, such as desorption electrospray ionization (DESI), direct analysis in real time (DART) and LAESI, has shown enhanced selectivity for the analysis of some pharmaceuticals and proteins.^{24–27} On-the-fly separation by IMS is especially important for untargeted metabolic analysis of single plant cells because of the large variety of isobaric chemical species present in them, and the limited cell volume available for analysis. However, single cell analysis using IMS-MS had not been demonstrated previously.

With different size, shape and functions, *Arabidopsis thaliana* (*A. thaliana*) epidermal cell types, such as pavement and basal cells, and trichomes, are interesting model systems for studying cellular growth, division and differentiation in plants.^{28–30} Phenotypic variations of whole plants and tissues are extensively studied on genetic level, whereas the metabolic makeup and pathways in the individual cell types of *A. thaliana* epidermis are less well understood.³¹ Sampling of the individual *A. thaliana* cell types presents challenges because the multiple cell types exhibit different morphologies, tensile strengths, and they coexist on the leaf epidermis. These plants present an additional technical challenge because their epidermis is too soft to be peeled off for producing a layer of pure epidermal cells without damage.

Capillary microsampling is a direct technique that utilizes a capillary tip to extract cell contents to be interrogated by various

detection methods, such as CE, real time PCR and MS, and also enables probing the metabolites located in specific regions of a cell.³² Analysis of different *A. thaliana* epidermal cell types in small populations of 200 cells was performed by capillary microsampling combined with gas chromatography (GC) MS.³³ The feasibility of live single cell MS, utilizing a nanospray tip for cell sampling coupled with MS detection, has been demonstrated for metabolite analysis of single cells in different organisms, such as isolated mammalian cells and tissue embedded plant cells.^{14–16,34–36} A similar technique, using a quartz capillary filled with an oil mixture, enabled the extraction and electrospray MS of single plant cells from tulip bulbs.³⁷ In order to enhance the molecular coverage in single cells and achieve a more detailed characterization of the metabolic variations between different *A. thaliana* epidermal cell types, a new analytical approach that directly links the single cell capillary microsampling with IMS and mass spectrometric analysis is needed.

Here we present a combination of capillary microsampling and ESI-IMS-MS for metabolic profiling of different *A. thaliana* epidermal cell types at the single cell level. We demonstrate that direct ESI of the extracted cell contents reduces the possibility of sample loss during handling leading to improved detection by MS. We also show that IMS can minimize the isobaric interferences and enhance the molecular coverage for single cells. Chemical structure identification was facilitated by tandem MS. The ion abundances corresponding to the metabolite levels in pavement and basal cells, and trichomes were differentiated on a single cell level.

Experimental

Chemicals

Methanol and water certified for HPLC were purchased from Alfa Aesar (Ward Hill, MA), whereas acetic acid ($\geq 99.0\%$ purity) was obtained from Fluka (St. Louis, MO). Electrospray solution was prepared by adding equal volumes of methanol and water and sufficient amount of acetic acid to reach a final concentration of 0.2% (v/v).

Plants

A. thaliana (Col-0) plants were grown in a growth chamber (PGC Flex, Conviron, Pembina, ND) at 70% humidity and a photoperiod alternating between 16 h of light (21 °C, 120 $\mu\text{E m}^{-2} \text{s}^{-1}$) and 8 h of dark (19 °C). After 4–6 weeks, healthy plants were used for our experiments. Entire leaves were cut from the plant and attached to clean microscope slides with double-sided tape.

Microcapillary fabrication

In order to penetrate the strong cell walls characteristic of plants, microsampling tips were custom-made using filamented borosilicate glass capillaries (BF100-50-10, Sutter Instrument, Novato, CA). The filament in the glass tube is needed to draw the electrospray solution to the tip of the needle by capillary action. The glass capillaries were fabricated by a P-97 micropipette puller (Sutter Instrument, Novato, CA) using a two-step

program. Due to their different geometries and wall strengths, pavement/basal cells and trichomes required specific micro-sampling capillaries. The parameter settings on the micropipette puller were adjusted depending on cell type to achieve the optimal extraction.

For the microsampling of *A. thaliana* pavement and basal cells, a capillary tip with a short taper and $\sim 1 \mu\text{m}$ opening was needed (see Fig. S1a in the ESI†). The parameter settings of the two-step pulling program for such a tip were: Step 1: Heat = 308, Pull = 40, Velocity = 30 and Time = 150, and Step 2: Heat = 310, Pull = 80, Velocity = 80 and Time = 120. Due to their larger size, stronger cell walls and different cell shape, trichomes required a capillary tip with a longer taper (see Fig. S1b in the ESI†). The parameter settings for these tips were: Step 1: Heat = 308, Pull = 40, Velocity = 30 and Time = 150, and Step 2: Heat = 310, Pull = 90, Velocity = 80 and Time = 110. A pair of pre-cleaned fine tweezers (no. 4, Dumont, Switzerland) was used to carefully break off the capillary tip to obtain a 5–10 μm opening at the end (see Fig. S1c in the ESI†). The parameter settings might vary for other micropipette pullers due to differences in the heating conditions.

Single cell sampling

Single cell capillary microsampling was performed by a motorized micromanipulator (TransferMan NK2, Eppendorf, Hauppauge, NY) mounted on a universal stand (Eppendorf, Hauppauge, NY) next to an upright microscope (Olympus BX51, Olympus Optical, Tokyo, Japan). A schematic view of the single

cell sampling setup is shown in Fig. 1a. A micropipette holder with a new capillary tip was attached to the micromanipulator at an angle of 0 and 10 degrees relative to the microscope sample stage for the trichomes and other cell types, respectively.

Initially, the capillary tip was moved into the focal plane of the microscope. Before sampling, it was moved $\sim 200 \mu\text{m}$ up to make room for the sample. Then the microscope slide with *A. thaliana* leaf was placed on the sample stage and brought to the focal plane. The cell of interest was centered in the field of view. At this point the capillary tip was carefully lowered and positioned to the centre of a single pavement or basal cell, or at the base of a single trichome. For microsampling of a single pavement or basal cell, the capillary tip was carefully inserted to a depth of $\sim 2 \mu\text{m}$ to prevent contact with the adjacent cells underneath. Insertion depth for the trichomes was less critical as they are larger and stand above the leaf surface. After the insertion of the tip, the cytoplasm automatically entered the sampling device driven by capillary action and turgor pressure. A manual air pump (CellTram, Eppendorf, Hauppauge, NY) was connected to the back of the capillary holder in case negative pressure was needed to harvest the cell contents.

ESI-IMS-MS

After extraction of the cell contents, the capillary was backfilled with 1 μl electrospray solution using a microloader pipette tip (cat no. 930001007, Eppendorf, Hauppauge, NY). The capillary was flicked on the side to remove small air bubbles before being attached to an electrode holder custom modified to have an insulating stem (H-12-S, Narishige, Tokyo, Japan). A platinum wire (diameter = 100 μm , Alfa Aesar, Ward Hill, MA) of $\sim 1.5 \text{ cm}$ in length was inserted into the capillary from the back end until it came in contact with the electrospray solution. The tip of the capillary was placed $\sim 5 \text{ mm}$ away from the orifice of a high resolution mass spectrometer (tuned to $\sim 10\,000$ FWHM resolution) equipped with a traveling wave (T-wave) based ion mobility separation (IMS) system (Synapt G2-S, Waters Co., Milford, MA) (see Fig. 1b). High voltage (2000 V) was applied to the wire by a power supply (PS350, Stanford Research Systems, Inc., Sunnyvale, CA) and an electrospray plume containing analyte particles was produced. The generated ions were initially retarded by collisions with the drift gas in the IMS system, separated according to their collision cross sections, and then transferred to the time of flight mass spectrometer for mass analysis. Nitrogen gas was used as the drift gas and supplied at a flow rate of 90 ml min^{-1} and a pressure of 3.25 mbar in the IMS system. The wave velocity and height in the IMS cell were optimized to 650 m s^{-1} and 40 V, respectively. The ion abundances as a function of drift time (DT) and mass-to-charge ratio (m/z) were recorded. Single cell spectra were averaged over 3 scans (1 scan/second). Structure identification was facilitated by tandem MS based on collision induced dissociation (CID) in Ar background gas at 20–30 eV energy.

Data analysis

The two-dimensional datasets were visualized by the DriftScope 2.4 software (Waters Co., Milford, MA) and the extracted mass

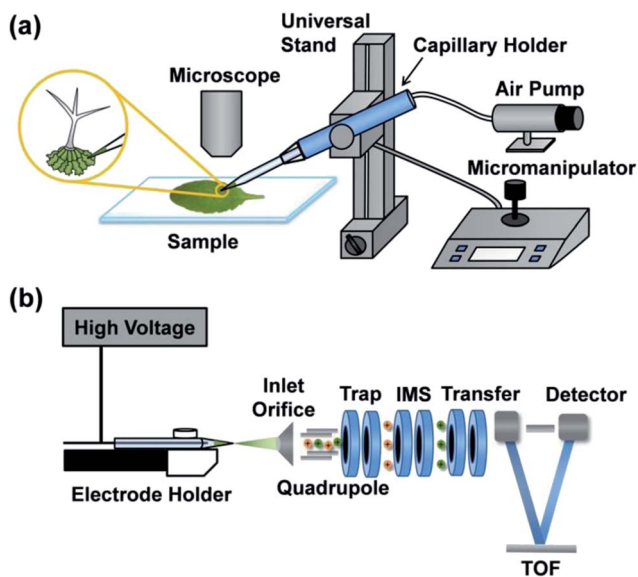


Fig. 1 (a) Schematic representation of single cell capillary micro-sampling. A capillary is held by a micromanipulator mounted on a universal stand next to a microscope. An air pump is utilized to apply negative pressure for extraction of the cell contents. (b) Schematic representation of ESI-IMS-MS analysis of the cell contents. A platinum wire is inserted into the sampling capillary and high voltage is applied. The produced ions are separated by an IMS system based on their collision cross sections, and subsequently analysed by a high resolution time-of-flight (TOF) mass spectrometer.

spectra were processed by the MassLynx 4.1 module (Waters Co., Milford, MA). The tentative identification of the ions was based on accurate mass measurements, and, for the abundant ions in the single cell spectra, on tandem MS. For the assignment of low abundance ions in the spectra, LAESI was performed on larger spots of the leaf combined with tandem MS.³⁸ All of the identified ions were also consistent with compounds found in a metabolite database specialized for *Arabidopsis* (AraCyc database from the Plant Metabolic Network <http://plantcyc.org>, last access on February 7, 2014). The NIST Isotope Calculator (ISOFORM, Version 1.02) was used to determine the theoretical monoisotopic masses.

Results and discussion

Capillary microsampling of single plant cells

Capillary tip diameter, shape (*e.g.*, tapering), and the insertion angle and position are critical for efficient and successful sampling of single cells. Due to their similar morphology, these parameters are the same for tissue embedded pavement and basal cells, however, they are significantly different for trichomes. Sequential images for capillary microsampling of these three cell types in the *A. thaliana* leaf are shown in Fig. 2. The two tissue-embedded cell types, pavement and basal cells, in the leaf were identified under an upright microscope and selected for microsampling by the capillary (see Fig. 2a and d). A capillary with a fine tip ($\sim 1 \mu\text{m}$ in diameter) was inserted into these cells for the extraction of the cell contents (see Fig. 2b and e). Due to the waxy cuticle present over the tissue embedded epidermal cells, the capillary tip is held at a shallow angle of 10° relative to the cell surface to effectively pierce the cuticle, and penetrate the cell wall and membrane. In *A. thaliana*, the volume of typical pavement and basal cells can be $\sim 20 \pm 3 \text{ pL}$,

whereas the volume of typical trichomes is $\sim 3.8 \pm 0.8 \text{ nL}$.³⁹ After $\sim 1 \text{ pL}$ of the basal or pavement cell contents was driven inside the tip by the turgor pressure and capillary action, the capillary was removed from the cell (see Fig. 2c and f). The extracted volume was estimated based on the meniscus position in the capillary. As it extends from the leaf surface and is much larger, the third cell type, the trichome (see Fig. 2g), required a different sampling strategy. A pulling protocol for a capillary with larger tip size ($5\text{--}10 \mu\text{m}$) and longer taper ($\sim 200 \mu\text{m}$) was developed. To minimize the bending of the trichome, the capillary insertion point was chosen close to its base (see Fig. 2h) and the insertion angle relative to the leaf surface was set to 0° . Due to its larger volume, extraction from a single trichome resulted in the removal of $\sim 5 \text{ pL}$ cell contents (see Fig. 2i).

Analysis of epidermal cell types

Initially we aimed at identifying the differences in the mass spectra for the three cell types. Single cell ESI-IMS-MS on the *A. thaliana* epidermis produced a cell specific signal for 3–5 s at the beginning of each measurement, followed by the electrospray background signal for another 10 s. Initially, to focus on mass analysis, spectra were obtained by integrating the signal for all DTs and the background spectra were subtracted. Representative mass spectra of single pavement and basal cells, and a trichome, are shown in Fig. 3a–c, respectively. Approximately

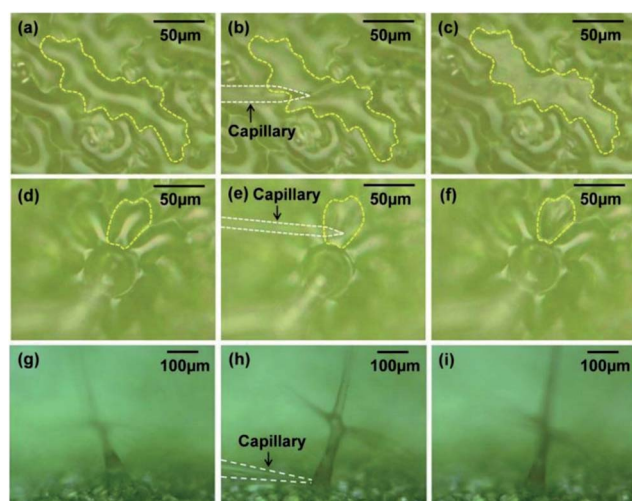


Fig. 2 Capillary microsampling process for single (a–c) pavement cells, (d–f) basal cells and (g–i) trichomes of *A. thaliana* observed under a microscope. The pavement and the basal cells are outlined by the yellow dashed line, whereas the capillary tip is indicated by the white dashed line. The three cell types are shown (a, d, g) before, (b, e, h) during and (c, f, i) after sampling.

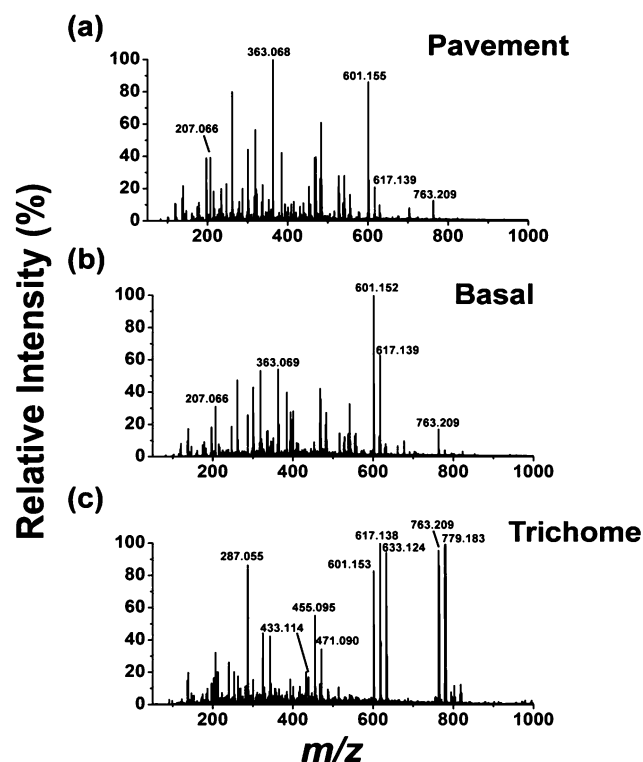


Fig. 3 Positive ion mass spectra of single *A. thaliana* epidermal cells: (a) pavement cell, (b) basal cell and (c) trichome, show distinct differences in their relative ion abundances.

200 peaks were detected in the spectrum of a single cell. Most peaks were distributed in the range of m/z 50–1000.

A list of the tentatively assigned metabolite ions are tabulated in Table S1 of the ESI.† The metabolite species labelled with “a” and “b” correspond to the ion assignments based on single cell tandem MS and LAESI tandem MS, respectively. Tandem MS and accurate mass matches were used for the identification of 21 metabolites and lipids, whereas another two metabolites were only tentatively identified based on the mass accuracy of the detected ions (<5 mDa).

Most of the identified ions fall in three compound classes, sinapic acid esters, *e.g.*, sinapoyl malate, flavonoids, *e.g.*, kaempferol glucoside, and phosphatidylcholine lipids, *e.g.*, PC (34 : 1). They are mainly detected in the sodium ion adduct form. To obtain a quantitative assessment of the differences in metabolic composition, we compared the intensities of specific ions in the three cell types. Mass spectra were collected from five cells of each cell type from the same plant, and were normalized based on their total ion counts. The ratio of the normalized intensities of a metabolite ion detected in trichomes and pavement cells, and in trichomes and basal cells were denoted as $I_{T:P}$ and $I_{T:B}$, respectively. When certain metabolite ions are present only in a single cell type, we use the symbols “T”, “B” and “P” instead of the intensity ratios for trichomes, basal cells, and pavement cells, respectively.

For example, the spectral features of small organic acids (*e.g.*, aconitic acid and sinapic acid) were common among all three cell types, and exhibited varying relative abundances. In contrast, sinapoyl glucose and phosphatidylcholines were not detected in the trichomes, whereas, kaempferol glucoside was absent in the spectra from pavement and basal cells.

Comparison of abundances for most flavonoid ions, such as the protonated kaempferol (m/z 287.055), and the sodium adduct of kaempferol rhamnoside (m/z 455.095), or their structural isomers, indicated $\sim 3 \times$ and $\sim 7 \times$ higher intensities, respectively, in the spectra obtained from trichomes. Sinapic acid (m/z 207.069) and its esters, such as sinapoyl malate (m/z 363.069), showed significantly higher levels, *i.e.*, $\sim 4 \times$ and $\sim 5 \times$, respectively, in the spectra of pavement and basal cells compared to trichomes.

Tandem MS was used to identify structural features of 21 ions. For example, the accurate masses of ions m/z 763 and m/z 779 are consistent with sodiated kaempferol triglycosides. Tandem mass spectra of the ions at nominal m/z 763 and m/z 779 produced from single trichomes are shown in Fig. S2 of the ESI,† with the assigned chemical structures presented in the insets. The major fragments of the precursor ion m/z 763, shown in Fig. S2a,† are m/z 617, due to the loss of one rhamnose residue, m/z 471, as a result of the loss of two rhamnose residues, and m/z 287, produced by the loss of all the glycones. Determination of the exact positions of all the glycone residues requires further analysis, typically by complementary methods, *e.g.*, HPLC or NMR, on bulk samples. Under the selected CID conditions, the m/z 287 fragment remained intact. Its accurate mass was consistent with kaempferol, luteolin or their structural isomers. Therefore when we mention kaempferol or its derivatives in this paper, we cannot exclude their structural

isomers. Review of the MetaCyc metabolic pathway database for *A. thaliana* indicates that kaempferol biosynthesis and the production of kaempferol-3-rhamnoside, kaempferol-3-rhamnoside-7-rhamnoside, kaempferol 3-O-sophoroside-7-O-rhamnoside, *etc.*, are active in this species (<http://www.metacyc.org/>, last accessed on March 31, 2014).

In Fig. S2b,† the major fragments of ion m/z 779, such as m/z 633, loss of a rhamnose residue, m/z 617, loss of a hexose (*e.g.*, glucose) residue, m/z 471, loss of a hexose (*e.g.*, glucose) and a rhamnose residues, and m/z 287, loss of all the glycones, resembles the fragmentation of m/z 763. As a result, the glycones attached to the flavonoid are tentatively identified as two rhamnose residues and one hexose residue for m/z 763, and one rhamnose residue and two hexose residues for m/z 779.

The relative intensities of 10 ions selected from Table S1† are compared in Fig. S3,† with the data corresponding to pavement and basal cells, and trichomes labelled in green, red and blue, respectively. The dashed line separates the sinapic acid, and its esters, from the flavonoid compound classes. The relative metabolite ion abundances exhibited different distributions in the two molecular groups. The relative abundances of m/z 207.069 (sinapic acid), m/z 363.069 (sinapoyl malate), and m/z 409.110 (sinapoyl glucose) were highest in pavement cells, followed by basal cells and lowest in trichomes. The relative abundances of the flavonoid ions shown in Fig. S3† were typically lowest in the pavement cells, followed by basal cells and highest in trichomes.

Enhanced analysis by ESI-IMS-MS

Retaining the DT information in the data enables the distinction of isobaric ions with differing collision cross sections, *e.g.*, structural isomers, and potentially improves the molecular coverage in the analysis of a single cell. The DT vs. m/z plot of a single pavement cell with the detected ions labelled by blue dots is shown in Fig. 4. In this plot, there were ~ 400 peaks associated with the cell material, a significant improvement over the ~ 200 peaks found in the mass spectrum of pavement cells (see Fig. 3a).

Sampling various subsections of the DT vs. m/z plot is a powerful way of selecting different compound classes and minimizing background interferences. For example in Fig. 4, the mass spectrum integrated over all the DTs (0–3.5 ms), presented in the inset with black frame, is dominated by the kaempferol triglycosides, other ions are suppressed and the overall signal-to-noise ratio is low. For comparison, the mass spectra in the m/z 750–800 range integrated over the DT = 1.8–2.3 ms, DT = 2.3–2.5 ms and DT = 2.5–2.7 ms are shown in panels with blue, yellow and red frames, respectively. Due to the separation according to DT, these three domains show dramatically different spectra. In the 2.3–2.5 ms and 2.5–2.7 ms ranges, ions tentatively assigned as kaempferol triglycosides or their isomers (inset in yellow frame), and nine phosphatidylcholine lipids (inset in red frame) are detected, respectively. These spectra are clearly separated according to the two compound classes with different collision cross sections. The third selected range, DT = 1.8–2.3 ms, presented in the panel

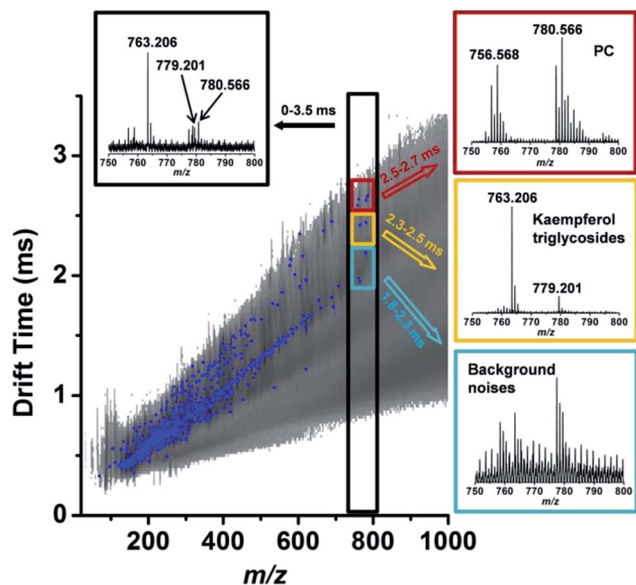


Fig. 4 DT vs. m/z plot of a single pavement cell. In the m/z 750–800 range, the mass spectra integrated over DT = 0–3.5 ms, DT = 1.8–2.3 ms, DT = 2.3–2.5 ms, and DT = 2.5–2.7 ms are shown with black, blue, yellow, and red frames, respectively. Compound classes with interfering mass spectra and background noise are distinguished by their drift times.

with blue frame, corresponds to a background noise that seems to be chemical in nature. Classes of molecular species with different collision cross sections, such as small metabolites, lipids and peptides, are displayed in different DT regions.^{40,41} For example, phosphatidylcholines with long acyl chains often display longer DT than metabolites of similar masses.

We also found that the IMS enhanced the dynamic range of the MS analysis of extracted cell contents. This is the consequence of separating the high intensity components and the chemical background in an m/z region from ions of low intensity (see the insets with yellow, red and blue frames in Fig. 4). Reduced interferences due to IMS can also facilitate the assignment of the detected ions because of unobscured isotope distribution patterns and simplified tandem MS spectra.

Comparing different regions within a DT vs. m/z plot can help with the classification of molecular groups. For example, in Fig. S4 of the ESI,† a DT vs. m/z plot of a single trichome is depicted with the framed regions assigned to mono-, di- and triglycosides of kaempferol based on the corresponding mass spectra (shown on the right). The DT vs. m/z plots are also helpful in the comparison of the metabolic makeup of different cell types. The phosphatidylcholine ions found at higher DT values for the pavement cells (see Fig. 4) were not detected in the trichomes, whereas the kaempferol glycoside ions were shown with much higher abundances in the latter.

Metabolic pathways

The abundances of many identified metabolites present in the three cell types of the *A. thaliana* epidermis were significantly different. The MetaCyc database (<http://metacyc.org/>, last

accessed on March 31st, 2014) was searched to identify the metabolic pathways related to the presence of the chemical species dominant in each cell type. Fig. S5 of the ESI† shows the relevant portion of the *A. thaliana* phenylpropanoid pathway, including three subpathways, *i.e.*, phenylpropanoid acid biosynthesis, kaempferol glycoside biosynthesis and sinapic acid ester biosynthesis, encompassing many of the identified metabolites. The metabolites that show significantly higher abundances in trichomes (framed in yellow) are all located in the kaempferol glycoside biosynthesis pathway, whereas the species that exhibit elevated levels in the pavement and basal cells (framed in blue) are found in the sinapic acid ester biosynthesis pathway.

Genetics studies have shown that flavonoids and sinapic acid esters are stored in *A. thaliana* leaves.⁴² Both of the sinapic acid esters and kaempferol glycosides are secondary metabolites that perform diverse functions in plants, for example they absorb UV radiation and mount a defence against pathogens.⁴³ Some other investigations have shown that anthocyanins, flavonoids and glucosinolates accumulate in the trichomes for plant defences and protection.⁴⁴ However, the localization of these metabolite classes in the three epidermal cell types is demonstrated for the first time at the single cell level in the present study.

Conclusions

In this contribution, we have shown the *in situ* metabolic analysis of single *A. thaliana* epidermal cell types, including pavement and basal cells, and trichomes, using capillary microsampling combined with ESI-IMS-MS. Metabolic differences were observed among the three different cell types and the specific metabolites accounting for most of variance in the mass spectra were identified. Significant enhancement was derived from the introduction of IMS resulting in the ability to distinguish isobaric or close to isobaric ions, *e.g.*, structural isomers, at the single cell level.

Distinguishing structural isomers is an important task in plant sciences where multiple isomers exist for important classes of metabolites with the same molecular weight. For example, alkaloids (*e.g.*, cathinone has four isomers in MetaCyc), flavonoids (*e.g.*, kaempferol glucoside has six isomers in AraCyc) and terpenes (*e.g.*, monoterpenes with C₁₀H₁₆ chemical formula have 33 structural isomers listed in MetaCyc) exhibit a large structural diversity. As long as the collision cross sections of the isomers are significantly different, the ESI-IMS-MS technique can provide important clues about which of them is present in the cell. Other techniques routinely used in distinguishing structural isomers, for example NMR spectroscopy, are not sufficiently sensitive to be of help at the single cell level.

Currently there are limitations on the selectivity of sampling subcellular contents, as the sampled material may or may not contain a particular organelle. Future implementations of the microsampling technique can benefit from combinations with non-destructive imaging techniques, such as fluorescence microscopy, and advanced imaging methods, such as coherent anti-Stokes Raman scattering microscopy, to identify

subcellular features of interest. Capillary microsampling with ESI-IMS-MS also has a potential to monitor metabolic changes in single cells during ontogenesis, or as a result of environmental stress. Other interesting directions include the investigation of cell-to-cell or subcellular metabolic gradients and single mammalian cell analysis.

Acknowledgements

This material is based upon work supported by the U.S. National Science Foundation under Grant no. CHE-1152302, and the George Washington University Selective Excellence Fund.

References

- 1 S. J. Altschuler and L. F. Wu, *Cell*, 2010, **141**, 559–563.
- 2 S. S. Rubakhin, E. V. Romanova, P. Nemes and J. V. Sweedler, *Nat. Methods*, 2011, **8**, S20–S29.
- 3 R. Zenobi, *Science*, 2013, **342**, 1243259.
- 4 A. Svatos, *Anal. Chem.*, 2011, **83**, 5037–5044.
- 5 R. A. Kruse, S. S. Rubakhin, E. V. Romanova, P. W. Bohn and J. V. Sweedler, *J. Mass Spectrom.*, 2001, **36**, 1317–1322.
- 6 S. G. Ostrowski, C. T. Van Bell, N. Winograd and A. G. Ewing, *Science*, 2004, **305**, 71–73.
- 7 S. G. Ostrowski, M. E. Kurczy, T. P. Roddy, N. Winograd and A. G. Ewing, *Anal. Chem.*, 2007, **79**, 3554–3560.
- 8 A. Amantonico, P. L. Urban, S. R. Fagerer, R. M. Balabin and R. Zenobi, *Anal. Chem.*, 2010, **82**, 7394–7400.
- 9 B. N. Walker, C. Antonakos, S. T. Retterer and A. Vertes, *Angew. Chem., Int. Ed.*, 2013, **52**, 3650–3653.
- 10 D. Holscher, R. Shroff, K. Knop, M. Gottschaldt, A. Creelius, B. Schneider, D. G. Heckel, U. S. Schubert and A. Svatos, *Plant J.*, 2009, **60**, 907–918.
- 11 J. H. Jun, Z. H. Song, Z. J. Liu, B. J. Nikolau, E. S. Yeung and Y. J. Lee, *Anal. Chem.*, 2010, **82**, 3255–3265.
- 12 I. Lanekoff, N. T. N. Phan, C. T. Van Bell, N. Winograd, P. Sjovald and A. G. Ewing, *Surf. Interface Anal.*, 2013, **45**, 211–214.
- 13 P. Nemes and A. Vertes, *TrAC, Trends Anal. Chem.*, 2012, **34**, 22–34.
- 14 H. Mizuno, N. Tsuyama, S. Date, T. Harada and T. Masujima, *Anal. Sci.*, 2008, **24**, 1525–1527.
- 15 N. Tsuyama, H. Mizuno, E. Tokunaga and T. Masujima, *Anal. Sci.*, 2008, **24**, 559–561.
- 16 T. Masujima, *Anal. Sci.*, 2009, **25**, 953–960.
- 17 S. Date, H. Mizuno, N. Tsuyama, T. Harada and T. Masujima, *Anal. Sci.*, 2012, **28**, 201–203.
- 18 S. C. Bendall, E. F. Simonds, P. Qiu, E. A. D. Amir, P. O. Krutzik, R. Finck, R. V. Bruggner, R. Melamed, A. Trejo, O. I. Ornatsky, R. S. Balderas, S. K. Plevritis, K. Sachs, D. Pe'er, S. D. Tanner and G. P. Nolan, *Science*, 2011, **332**, 687–696.
- 19 B. Shrestha and A. Vertes, *Anal. Chem.*, 2009, **81**, 8265–8271.
- 20 B. Shrestha, P. Nemes and A. Vertes, *Appl. Phys. A*, 2010, **101**, 121–126.
- 21 B. Shrestha, J. M. Patt and A. Vertes, *Anal. Chem.*, 2011, **83**, 2947–2955.
- 22 J. A. Stolee, B. Shrestha, G. Mengistu and A. Vertes, *Angew. Chem., Int. Ed.*, 2012, **51**, 10386–10389.
- 23 J. T. Aerts, K. R. Louis, S. R. Crandall, G. Govindaiah, C. L. Cox and J. V. Sweedler, *Anal. Chem.*, 2014, **86**, 3203–3208.
- 24 D. J. Weston, R. Bateman, I. D. Wilson, T. R. Wood and C. S. Creaser, *Anal. Chem.*, 2005, **77**, 7572–7580.
- 25 S. Myung, J. M. Wiseman, S. J. Valentine, Z. Takats, R. G. Cooks and D. E. Clemmer, *J. Phys. Chem. B*, 2006, **110**, 5045–5051.
- 26 M. D. Likar, G. L. Cheng, N. Mahajan and Z. L. Zhang, *J. Pharm. Biomed. Anal.*, 2011, **55**, 569–573.
- 27 B. Shrestha and A. Vertes, *Anal. Chem.*, 2014, **86**, 4308–4315.
- 28 S. Guimil and C. Dunand, *J. Exp. Bot.*, 2007, **58**, 3829–3840.
- 29 M. Andriankaja, S. Dhondt, S. De Bodt, H. Vanhaeren, F. Coppens, L. De Milde, P. Muhlenbock, A. Skirycz, N. Gonzalez, G. T. S. Beemster and D. Inze, *Dev. Cell*, 2012, **22**, 64–78.
- 30 S. Dhondt, N. Wuyts and D. Inze, *Trends Plant Sci.*, 2013, **18**, 433–444.
- 31 X. B. Dai, G. D. Wang, D. S. Yang, Y. H. Tang, P. Broun, M. D. Marks, L. W. Sumner, R. A. Dixon and P. X. Zhao, *Plant Physiol.*, 2010, **152**, 44–54.
- 32 A. D. Tomos and R. A. Sharrock, *J. Exp. Bot.*, 2001, **52**, 623–630.
- 33 B. Ebert, D. Zoller, A. Erban, I. Fehrlé, J. Hartmann, A. Niehl, J. Kopka and J. Fisahn, *J. Exp. Bot.*, 2010, **61**, 1321–1335.
- 34 H. Mizuno, N. Tsuyama, T. Harada and T. Masujima, *J. Mass Spectrom.*, 2008, **43**, 1692–1700.
- 35 M. L. Tejedor, H. Mizuno, N. Tsuyama, T. Harada and T. Masujima, *Anal. Sci.*, 2009, **25**, 1053–1055.
- 36 M. L. Tejedor, H. Mizuno, N. Tsuyama, T. Harada and T. Masujima, *Anal. Chem.*, 2012, **84**, 5221–5228.
- 37 Y. Gholipour, R. Erra-Balsells, K. Hiraoka and H. Nonami, *Anal. Biochem.*, 2013, **433**, 70–78.
- 38 P. Nemes and A. Vertes, *Anal. Chem.*, 2007, **79**, 8098–8106.
- 39 G. Gutierrez-Alcala, C. Gotor, A. J. Meyer, M. Fricker, J. M. Vega and L. C. Romero, *Proc. Natl. Acad. Sci. U. S. A.*, 2000, **97**, 11108–11113.
- 40 S. N. Jackson, H. Y. J. Wang and A. S. Woods, *J. Am. Soc. Mass Spectrom.*, 2005, **16**, 133–138.
- 41 J. A. McLean, B. T. Ruotolo, K. J. Gillig and D. H. Russell, *Int. J. Mass Spectrom.*, 2005, **240**, 301–315.
- 42 J. J. Sheahan, *Am. J. Bot.*, 1996, **83**, 679–686.
- 43 A. K. Bharti and J. P. Khurana, *Photochem. Photobiol.*, 1997, **65**, 765–776.
- 44 M. J. Jakoby, D. Falkenhan, M. T. Mader, G. Brininstool, E. Wischnitzki, N. Platz, A. Hudson, M. H. R. Lskamp, J. Larkin and A. Schnittger, *Plant Physiol.*, 2008, **148**, 1583–1602.

Electronic Supplementary Information for

**In Situ Metabolic Analysis of Single Plant Cells by Capillary
Microsampling and Electrospray Ionization Mass Spectrometry
with Ion Mobility Separation**

Linwen Zhang,^a Daniel P. Foreman,^a Paaqua A. Grant,^b Bindesh Shrestha,^a Sally A. Moody,^c Florent
Villiers,^d June M. Kwak^e and Akos Vertes*^a

^a*Department of Chemistry, W. M. Keck Institute for Proteomics Technology and Applications, The George Washington University, Washington, DC 20052, USA*

^b*Department of Biological Sciences, The George Washington University, Washington, DC 20052, USA*

^c*Department of Anatomy and Regenerative Biology, The George Washington University, Washington, DC 20037, USA*

^d*Department of Cell Biology and Molecular Genetics, University of Maryland, College Park, Maryland 20742, USA*

^e*Center for Plant Aging Research, Institute for Basic Science, Department of New Biology, Daegu Gyeongbuk Institute of Science and Technology, Daegu 711-873, Republic of Korea*

*Corresponding author. E-mail: vertes@gwu.edu, Phone: +1 (202) 994-2717, Fax: +1 (202) 994-5873.

Fig. S1 Capillaries for sampling of (a) pavement or basal cells, and trichomes (b) before cutting and (c) after cutting. The insets show the capillary tips at higher magnifications (inset scale bars are 10 μm). The tip diameters are $\sim 0.7 \mu\text{m}$, $\sim 0.2 \mu\text{m}$, and $\sim 5 \mu\text{m}$, respectively.

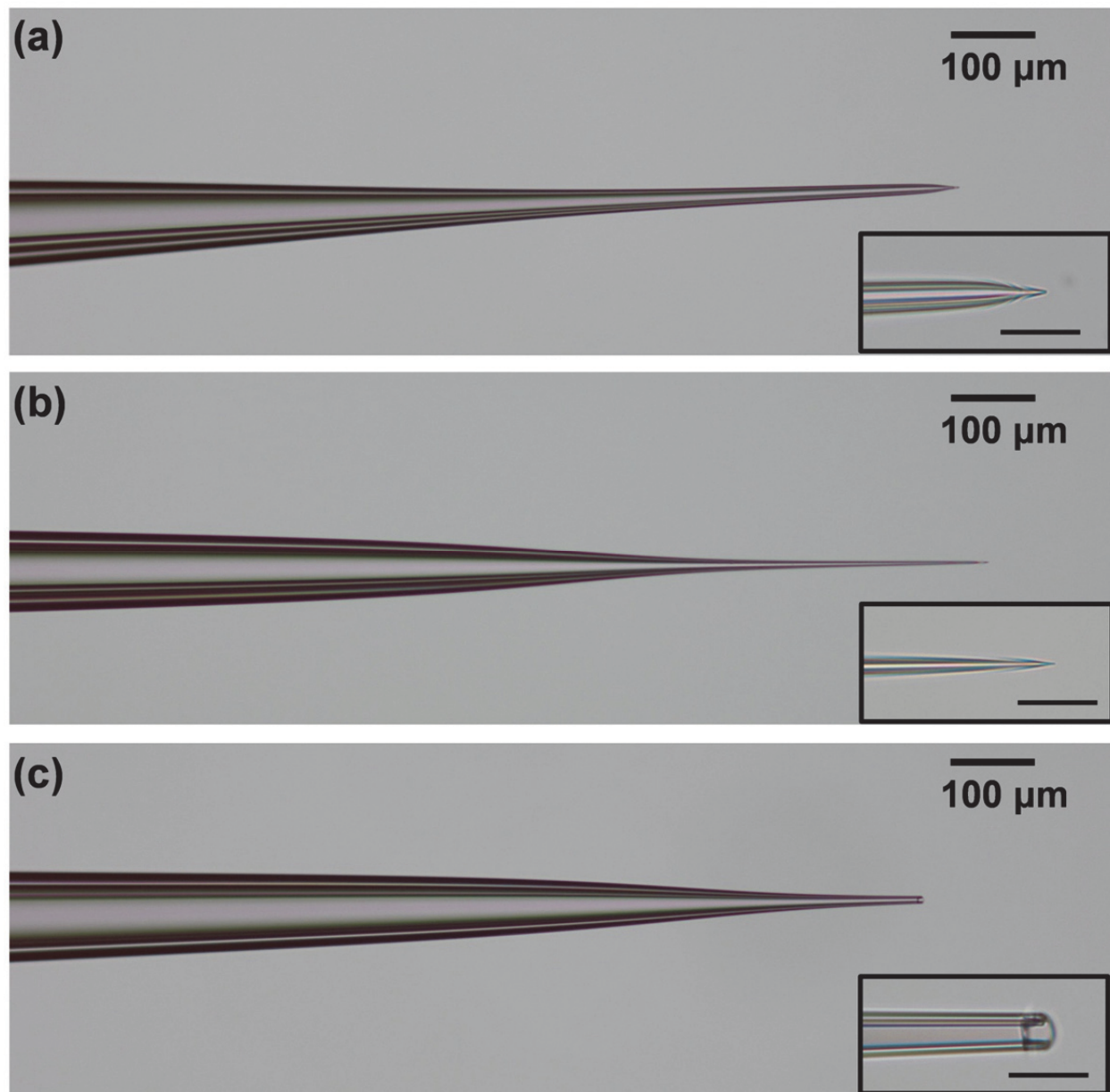


Fig. S2 Single cell tandem mass spectra of ions (a) m/z 763 and (b) m/z 779, with corresponding structures. In spectrum (a), the fragments m/z 287.056, 471.081, and 617.149 are derived from the m/z 763.217 precursor ion by loss of all the glycones, two rhamnosides, and one rhamnoside, respectively. In spectrum (b), the precursor ion, m/z 779.181, fragments to produce m/z 287.055, 471.079, 617.137, and 633.124 by the loss of all glycones, one glucoside and one rhamnoside, one glucoside, and one rhamnoside, respectively.

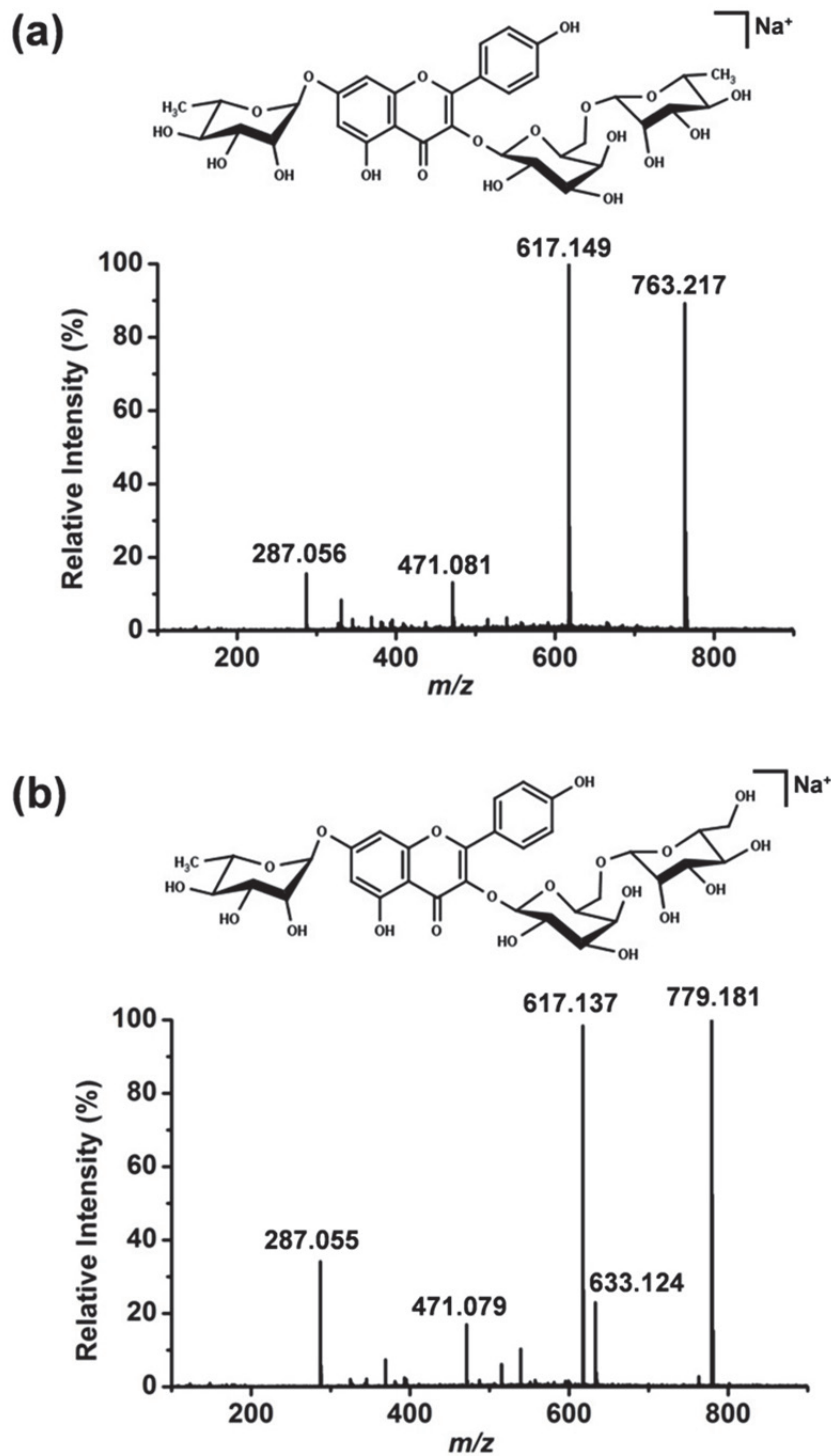


Fig. S3 Normalized intensities of selected metabolite ions detected in pavement cells (green), basal cells (red) and trichomes (blue). K, Rha and Glc denote kaempferol, rhamnoside and glucoside, respectively. Sinapic acid esters and kaempferol glycosides are separated by a dashed line. Significantly different metabolite levels are observed in the three cell types.

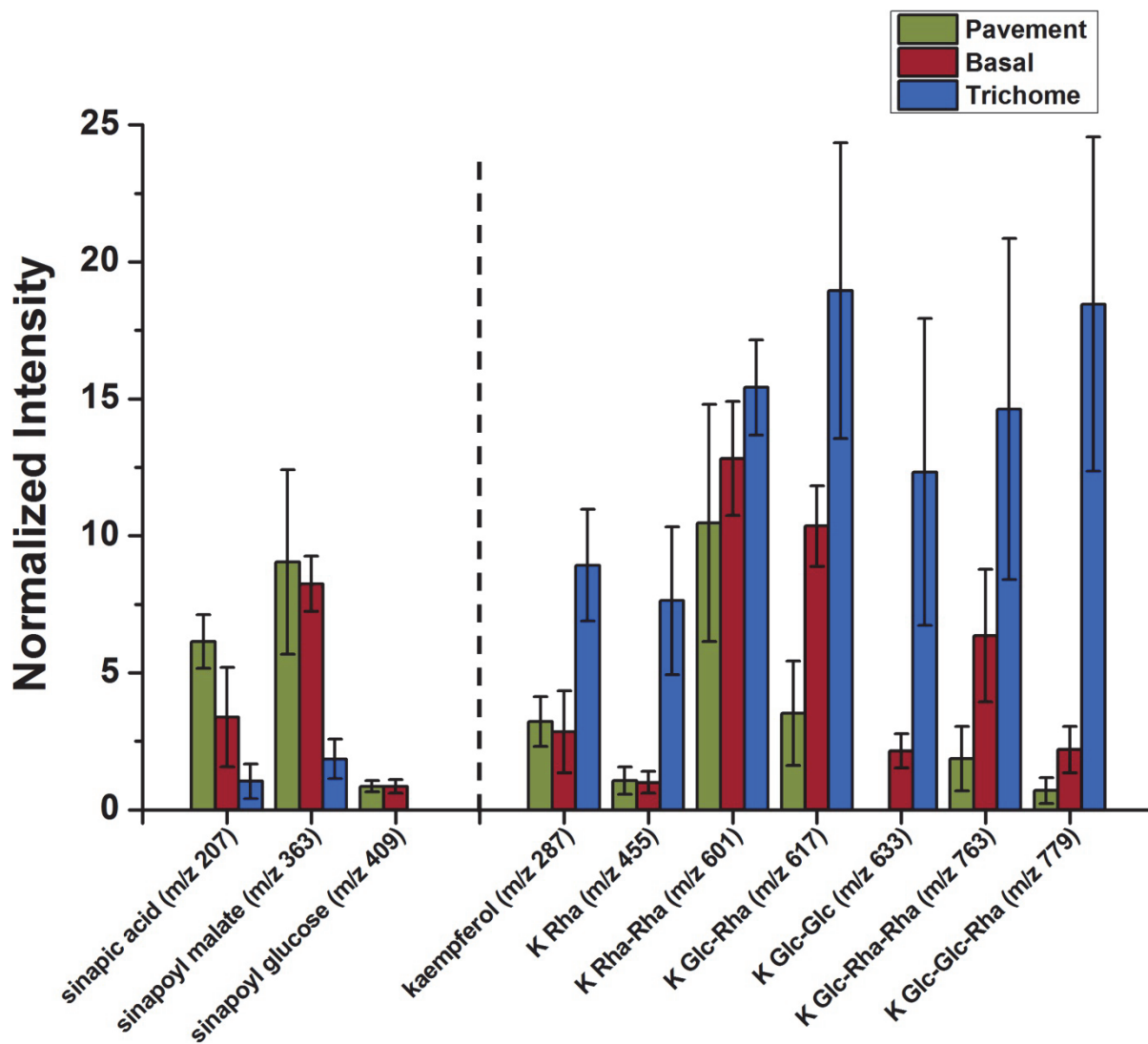


Fig. S4 A DT vs. m/z plot produced by the analysis of a single trichome using capillary microsampling ESI-IMS-MS. The mass spectra shown on the right, corresponding to the framed regions in the 2D plot, indicate the presence of mono-, di- and triglycosides of kaempferol (K).

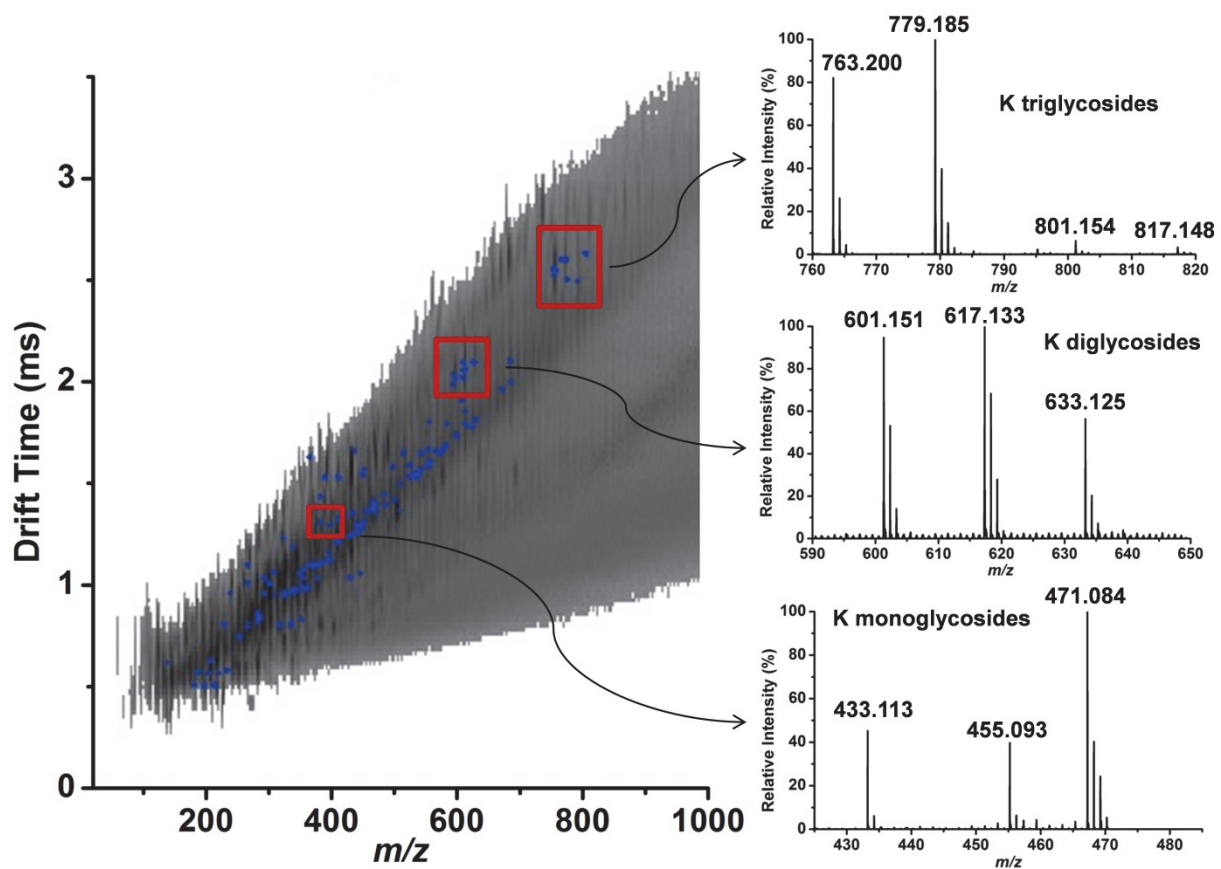


Fig. S5 Part of phenylpropanoid metabolism pathways in *A. thaliana* with the phenylpropanoid acid biosynthesis, sinapic acid ester biosynthesis, and kaempferol glycoside biosynthesis subpathways framed by dashed rectangles (K = kaempferol, Rha = rhamnoside and Glc = glucoside). Metabolites detected at higher levels in pavement and basal cells, and in trichomes are marked by blue and yellow frames, respectively. The detected ions are indicated by the measured m/z values.

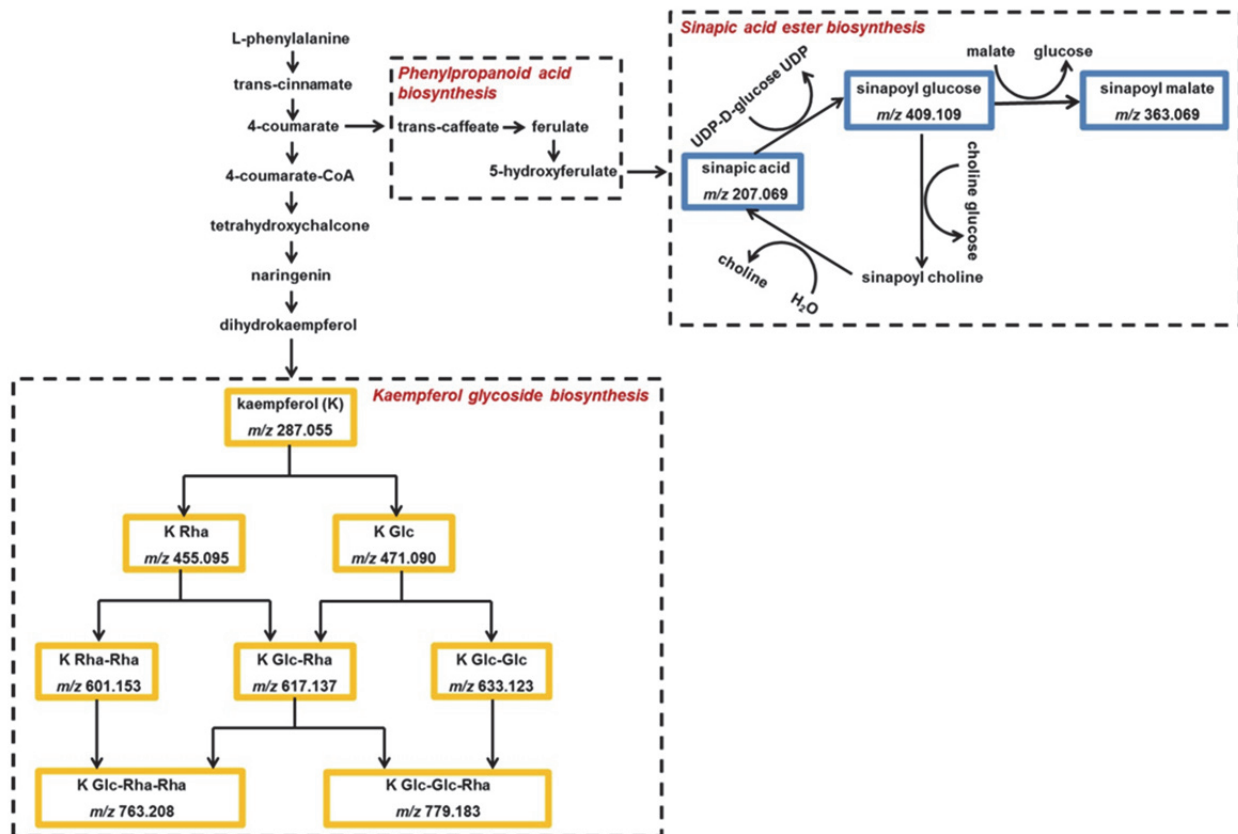


Table S1. Tentative assignments of metabolite ions detected in the three *A. thaliana* epidermal cell types. The ratios of the normalized ion abundances from trichomes and pavement cells ($I_{T:P}$), and from trichomes and basal cells ($I_{T:B}$) are shown. Symbols “T”, “P” and “B” indicate that the ion was only detected in trichomes, pavement cells or basal cells, respectively.

Compound	Formula	Measured Mass	Calculated Mass	Δm (mDa)	$I_{T:P}$	$I_{T:B}$
coumarin	C ₉ H ₆ O ₂	147.046 (+H ⁺)	147.0441	1.9	0.15	0.47
aconitic acid ^b	C ₆ H ₆ O ₆	175.038 (+H ⁺)	175.0237	14.3	0.15	0.27
sinapic acid ^b	C ₁₁ H ₁₂ O ₅	207.069 (-H ₂ O+H ⁺) 247.049 (+Na ⁺) 263.024 (K ⁺)	207.0652 247.0577 263.0316	3.8 -8.7 -7.6	0.17 P P	0.31 B B
kaempferol ^c	C ₁₅ H ₁₀ O ₆	287.055 (+H ⁺) 325.003 (+K ⁺)	287.0550 325.0109	0 -7.9	2.77 T	3.13 T
sinapoyl malate ^b	C ₁₅ H ₁₆ O ₉	363.069 (Na ⁺)	363.0686	0.4	0.20	0.22
disaccharide ^b	C ₁₂ H ₂₂ O ₁₁	365.113 (+Na ⁺) 381.078 (+K ⁺)	365.1054 381.0794	7.6 -1.4	0.75 0.87	0.24 0.14
sinapoyl glucose ^b	C ₁₇ H ₂₂ O ₁₀	409.110 (Na ⁺)	409.1105	-0.5	P	B
kaempferol rhamnoside ^{a,d}	C ₂₁ H ₂₀ O ₁₀	433.114 (+H ⁺) 455.095 (+Na ⁺)	433.1129 455.0949	1.1 0.1	T 7.13	T 7.63
kaempferol glucoside ^{a,d}	C ₂₁ H ₂₀ O ₁₁	471.090 (+Na ⁺)	471.0898	0.2	T	T
kaempferol dirhamnoside ^{a,d}	C ₂₇ H ₃₀ O ₁₄	601.153 (+Na ⁺)	601.1528	0.2	1.47	1.20
kaempferol glucoside-rhamnoside ^{a,d}	C ₂₇ H ₃₀ O ₁₅	617.137 (+Na ⁺)	617.1477	-10.7	5.38	1.83
kaempferol diglucoside ^{a,d}	C ₂₇ H ₃₀ O ₁₆	633.123 (+Na ⁺)	633.1426	-19.6	T	5.71
PC (34:4) ^b	C ₄₂ H ₇₆ NO ₈ P	754.552 (+H ⁺)	754.5381	13.9	P	B
PC (34:3) ^b	C ₄₂ H ₇₈ NO ₈ P	756.568 (+H ⁺) 794.510 (+K ⁺)	756.5538 794.5096	14.2 0.4	P P	B B
PC (34:2) ^b	C ₄₂ H ₈₀ NO ₈ P	758.581 (+H ⁺) 796.526 (+K ⁺)	758.5694 796.5253	11.6 0.7	P P	B B
PC (34:1) ^b	C ₄₂ H ₈₂ NO ₈ P	760.597 (+H ⁺)	760.5851	11.9	P	B
kaempferol glucoside-rhamnoside ^{a,d}	C ₃₃ H ₄₀ O ₁₉	763.208 (+Na ⁺) 801.162 (-H ⁺ +Na ⁺ +K ⁺)	763.2056 801.1615	2.4 0.5	7.84 T	2.30 T
PC (36:6) ^b	C ₄₄ H ₇₆ NO ₈ P	778.549 (+H ⁺)	778.5381	10.9	P	B
kaempferol glucoside-glucoside-rhamnoside ^{a,d}	C ₃₃ H ₄₀ O ₂₀	779.183 (+Na ⁺) 817.157 (-H ⁺ +Na ⁺ +K ⁺)	779.2005 817.1564	-17.5 0.6	26.17 T	8.39 T
PC (36:5) ^b	C ₄₄ H ₇₈ NO ₈ P	780.566 (H ⁺) 802.552 (Na ⁺)	780.5538 802.5357	12.2 16.3	P P	B B
PC (36:4) ^b	C ₄₄ H ₈₀ NO ₈ P	782.580 (H ⁺) 804.559 (Na ⁺)	782.5694 804.5513	10.6 7.7	P P	B B
PC (36:3) ^b	C ₄₄ H ₈₂ NO ₈ P	784.597 (H ⁺) 806.578 (Na ⁺)	784.5851 806.5670	11.9 11.0	P P	B B
PC (36:2) ^b	C ₄₄ H ₈₄ NO ₈ P	786.601 (H ⁺) 808.580 (Na ⁺)	786.6007 808.5826	0.3 -2.6	P P	B B

^aChemical species assigned based on tandem MS from capillary microsampling of single cell.

^bChemical species assigned based on tandem MS from LAESI of multiple cells.

^cKaempferol and its structural isomers are consistent with the measured m/z .

^dKaempferol and its structural isomers are consistent with the tandem MS data.